Indian Journal of Engineering & Materials Sciences
Vol. 27, April 2020, pp. 344-347

Tensile fracture behavior of high carbon high manganese steel with single-phase austenite structure

Zhimin Ding[a]*, Jiaqi Li[a] & Rui Feng[b]

[a]College of Materials Science and Engineering, Dalian Jiaotong University, Dalian, Liaoning 116028, China
[b]CRRC Datong Co., Ltd, Datong, Shanxi 037038, China

Received: 22 November 2016; Accepted: 13 August 2018

The microstructure, fracture morphology and tensile fracture process of high manganese steel with single-phase austenite after water toughening have been investigated by optical microscope (OM), scanning electron microscope (SEM) and transmission election microscope (TEM). The results have shown a large number of deformation twins forming within the austenite matrix after tensile fracture, which have been parallel with and cross to each other. The fracture surface has in the shape of dimple and parallel cascade steps inside the larger size. There has been existed many Shockley partial dislocations, stacking faults and dislocation loops at twin-twin intersections. We have discovered like-microvoid accumulation fracture caused by non-second-phase particles in high manganese steel with single-phase austenite, and the reasons for its formation have been discussed in this paper.

Keywords: High carbon high manganese steel, Single-phase austenite, Microvoid, Dimple

1 Introduction

It is well known that high carbon high manganese steel has high toughness and an excellent work hardening ability, even excellent wear resistance after water toughening treatment, which is wildly used in railway, mining, building materials and other industries[1,2]. Meanwhile, high manganese steel possesses the typical characteristics of ductile fracture consisting of voids nucleation, growth and coalescence due to its high plasticity and toughness, and shows dimple morphology in the micro-fracture surface. Similarly, the studies of literatures[3-5] about fracture morphology of high manganese steel also resulted in a similar observation. In general, dimple morphology of fracture is often observed in the common metal materials with many second particles in the matrix and the microvoids nucleation sites are easy to be located at second-phase precipitates, especially in the precipitates at grain boundaries[6-8] and larger grain boundaries[9]. In addition, for high carbon high manganese steel treated by aging treatment, D.Rittel[3] and SF Gnyusov[10] also observed a large number of dimples on the tensile fracture surface, they confirmed that dimples are formed by holes first forming in the second-phase precipitates, then growing up and coalescing, and finally developing a continuous fracture surface under the combined influence of plastic deformation and stress state. Therefore, it can be concluded that the formation of micro-fracture morphology of dimple is associated with the second-phase particles in the matrix through the study above, but for single phase with no precipitates, such as high carbon high manganese steel with single-phase austenite after water toughening treatment, the reasons about its dimple forming have hardly been reported. Rudd[11] proposed that the nucleation would occur when the local stress at trigeminal grain boundaries exceeds a certain amplitude of the material, and with the increase of loading strain rate, the nucleation rate is also raised basing on the atomic simulation of nano-voids dynamic evolution in polycrystalline copper. But it has not been confirmed by experiments that the nucleation of microvoids is at trigeminal grain boundaries. So, in order to clarify the position of dimple nucleation in single-phase structure, the microstructure and morphology of high carbon high manganese steel with single-phase austenite after tensile fracture were investigated.

2 Experimental Materials and Methods

100Mn13 high manganese steel was used in this study, and its chemical composition is given in Table 1. The experimental 100Mn13 steel was forged into a bar with diameter of 70mm after smelting and

*Corresponding author (E-mail: dingzm@djtu.edu.cn)

Table 1 — Chemical composition of experimental steels (mass fraction, %)

Ingredient	C	Mn	Si	S	P
Content/Wt%	1.00	12.89	0.53	0.006	0.023

casting followed by wire cutting into a diameter of 30 mm. In order to get homogeneous single-phase austenite, the specimen was prepared by water toughening treatment at 1323 K for 2 h.

Tensile tests were performed on WEW-600 universal testing machine at room temperature. The experimental specimen was standard cylindrical rod with a diameter of 20 mm. The metallographic specimen selected from longitudinal section of fracture cylindrical rod were prepared by mechanical grinding, polishing and then corroding with the alcohol solution containing 4% of nitric acid (volume fraction) and hydrochloric acid solution. The specimen for SEM was obtained from 10~15 mm under the fracture surface. Thin foils for TEM were prepared by grinding the sheets to approximately 30 μm thickness followed by wire cutting into 0.5mm thickness and punching discs with a diameter of 3mm, and then perforating by ion milling. The microstructure of 100Mn13 high manganese steel was observed by a NEOPHOT21 optical microscope, a SUPRA55 scanning electron microscope and a JEM-2100F TEM operating at 200 kv.

3 Results and Analysis

3.1 Metallographic structure of 100Mn13 steel before and after tensile test

Figures 1 and 2 are metallographic images of 100Mn13 steel treated by water toughening treatment before and after tensile test. It shows that before tensile test homogeneous single-phase austenite is obtained by water toughening treatment, and no second-phase particles or carbides precipitate at trigeminal grain boundaries in Fig. 1b. While after tensile test, there are a large number of deformation twins in austenite grains and each grain includes not only initial twins, but also the secondary twins which have a certain angle of intersection with initial ones, as shown by the arrow A in Fig. 2a, and most of twins end in the grain boundary. In Fig. 2b, microcracks formed by the accumulation and aggregation of microvoids mainly nucleate at twin boundaries, and most of them extend along the twin boundaries as shown in B. Because of high stability and low fault energy of austenite structure[12,13], no particles precipitated and twinning is one of the primary plastic deformation modes in 100Mn13 steel during the deformation and fracture process.

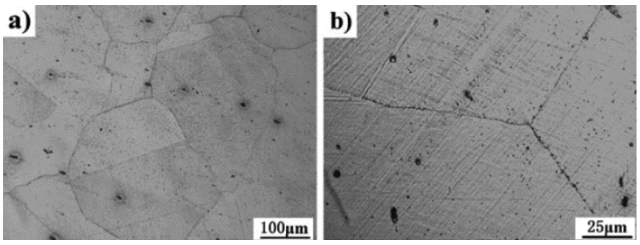

Fig. 1 — Metallographic images of 100Mn13 steel treated by water toughening (a) single-phase austenite and (b) high magnification about trigeminal grain boundaries.

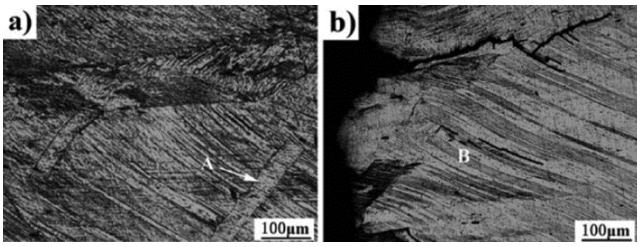

Fig. 2 — Metallographic images of 100Mn13 steel treated by water toughening after tensile test (a) deformation twins in austenite grains and (b) microcracks nucleate at twin boundaries.

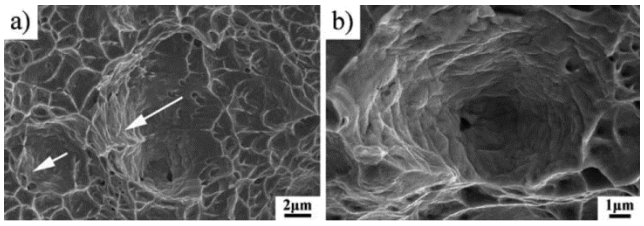

Fig. 3 — Fracture morphology of 100Mn13 steel (a) fracture morphology of the dimple and (b) enlarged image of the dimple in (a).

3.2 Fracture morphology of 100Mn13 steel observed by SEM

Figure 3 illustrates the fracture morphology of 100Mn13 steel with single-phase austenite after tension fracture. It obviously shows that there exist many dimples of similar sizes and a small amount of larger ones in the fracture surface, and a lot of roughly parallel cascade steps are observed in the interior of some great dimples through careful observation, as shown by the arrow in Fig. 3a and 3b. In addition, different from structural steels, second-phase particles or inclusions are not seen in the dimples at the fracture surface of high manganese steel.

3.3 Microstructure of 100Mn13 steel after tensile fracture observed by TEM

Figure 4 gives microstructure of 100Mn13 steel after tensile fracture and its selected-area diffraction pattern observed by TEM. It shows that the diffraction

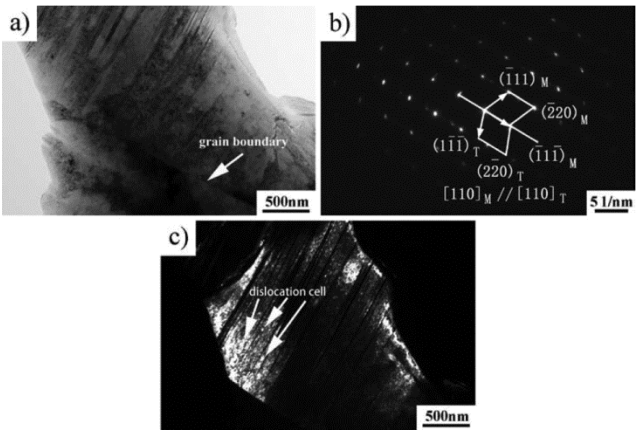

Fig. 4 — TEM micrograph and diffraction pattern of 100Mn13 steel after tension fracture (a) TEM micrograph of twin-grain boundary intersection, (b) selected-area diffraction pattern and (c) dark field image of matrix.

pattern of deformation twin possess the characteristics of typical face centered cubic crystal structure, its twinning plane is $(\bar{1}1\bar{1})$ and direction is $[\bar{1}12]$, as shown in Fig. 4b. Moreover, many dislocation cells which are developing by that a large number of dislocations tangle mutually exist on both sides of the grain boundary, especially in the area where twin and grain boundary intersect, which can be seen in the TEM dark field images of matrix shown in Fig. 4c.

Figure 5 shows the TEM micrograph (lower left corner) and HRTEM atomic lattice image of the twin-twin intersection. The relationship between twin boundary 1 (TB1) and twin boundary 2 (TB2) is confirmed by the fast Fourier transformation of the lattice image shown in the lower right corner. The two white broken lines represent TB1 and TB2, respectively. In addition, partial dislocation is marked by T and its bottom line indicates the stacking fault by the motion of partials. The two T circled by dashed ring compose of dislocation loops formed by Shockley partial dislocations in two opposite directions. As can be seen from HRTEM image, different from other locations, there present a serious distortion and a large number of partial dislocations, stacking faults and dislocation loops with inner vacancies at twin-twin intersection. According to Burgers Circuit, the Shockley partial dislocation formed at intersection is edge type. By analyzing the atomic lattice image and its selected-area diffraction pattern, the twin plane of twin 1 and twin 2 are $(1\bar{1}\bar{1})$ and $(1\bar{1}1)$. As we all know, Shockley partial dislocations can only slide in {111} plane and its direction is $<\bar{2}11>$ in fcc metals, so partials and

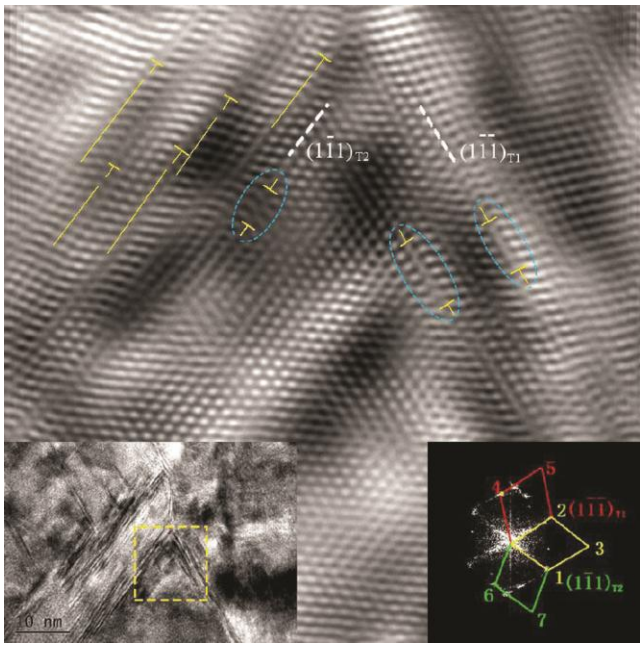

Fig. 5 — HRTEM image of twin-twin intersection.

dislocation loops are pinned crystal defects in {110} plane which are perpendicular to {111} plane. For the pinned dislocations at twin-twin intersection mentioned above, they may become the cores of the microvoids.

4 Discussion

As shown in 3.2 section, there exist many dimples of similar sizes and a small amount of larger ones in fracture surface, and a lot of roughly parallel cascade steps at the interior of larger dimples. While, the reason about these fracture morphologies forming in single-phase austenite with no second particles have hardly been reported before. It been thought to be related to the partial dislocations, stacking faults and dislocation loops at twin-twin intersections or twin-grain boundary intersections in the tensile fracture process by this paper.

When the deformation reaches a certain degree, crystal defects such as partial dislocations, stacking faults and dislocation loops can be generated at intersections as shown in Fig. 5. In addition, partials and dislocation loops cannot move under the stress. It is conceivable that with the extension of deformation, the new partials and dislocation loops will come into being continuously close to the original ones, then all of them can combine, and corresponding microvoids may form respectively. After nucleating, microvoids will grow up constantly and connect with each other

in the following deformation process, eventually result in the fracture and showing dimple fracture morphology. The microvoids nucleation mechanism is proposed in Fig. 6 and 7.

When 100Mn13 steel is subjected to axial tensile loads, partial dislocations form at twin-twin intersections or twin-grain boundary intersections as shown in Fig. 6(a). And with deforming continually, a large number of partials assemble as well as merge with each other at the intersection, and finally microvoids nucleate as shown in Fig. 6(b). In addition, much dislocation loops with inner vacancies will generate during the tensile test as shown in Fig. 7(a). With the deformation increasing, dislocation loops gather together and a large vacancy sheet formed by the aggregation of vacancies in dislocation rings, finally, the space sheet continues to thicken or mutually merge to form a microvoid under the stress, as shown in Fig. 7(b). We can assume that when the twin boundaries slide directly into the larger dimple, lots of roughly parallel cascade steps on its inner wall can come into being, which may form the morphology as shown in Fig. 8.

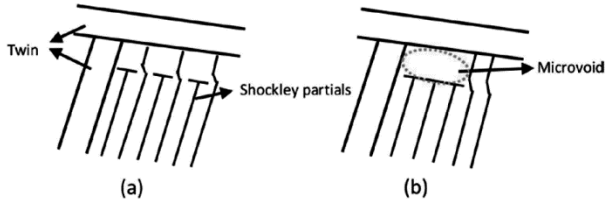

Fig. 6 — Schematic diagram of microvoid formation mechanism by Shockley partial dislocations (a) Shockley partial dislocations gathered at twin-twin intersection and (b) Shockley partial dislocations coalescence to form a dimple.

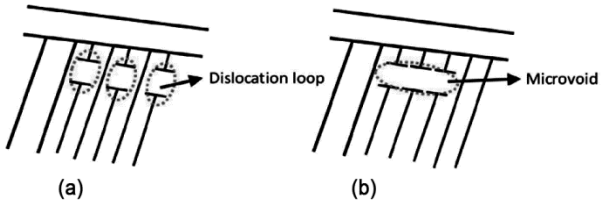

Fig. 7 — Schematic diagram of microvoid formation mechanism by dislocation loops (a) dislocation loops gathered at twin-twin intersection and (b) dislocation loops coalescence to form a dimple.

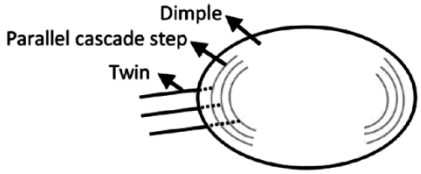

Fig. 8 — Dimple with parallel cascade steps.

However, previous works[14,15] reported that, microvoids were formed by breaking the second-phase particles or separating particles and matrix at the interface in common structural steels. Because microvoid formation method proposed by the paper is different from the one proposed by previous works, the fracture caused by partial dislocations and dislocation loops and not by second-phase particles is proposed as the like-microvoid accumulation fracture method by this paper.

5 Conclusions

In summary, the microstructure, fracture morphology and tensile fracture process of high manganese steel with single-phase austenite have been investigated in this paper. The results are as follows: there are a large number of deformation twins in austenite matrix which are parallel with and cross to each other. The fracture surface is in the shape of dimple and has parallel cascade steps inside the larger size. Many Shockley partial dislocations, stacking faults and dislocation loops formed at twin-twin intersections. In addition, we have proposed two microvoid formation mechanisms for single-phase austenite in high manganese steel, which including Shockley partial dislocations coalesce and dislocation loops coalesce, respectively at twin-twin intersections.

References

1 Dastur Y N & Leslie W C, *Metall Mater Trans A*, 12 (1981) 749.
2 Karaman I, Sehitoglu H, Beaudoin A J, Chumlyakov Y I, Maier H J & Tome C N, *Acta Mater*, 48 (2000) 2031.
3 Rittel D & Roman I, *Metall Mater Trans A*, 19 (1988) 2269.
4 Bayraktar E, Khalid F A & Levaillant C, *J Mater Process Tech*, 147 (2004) 145.
5 Hamada A S, Karjalainen L P & Somani M C, *Mater Sci Eng A*, 467 (2007) 114.
6 Qiu H, Mori H, Enoki M & Kishi T, *ISIJ Int*, 39 (1999) 358.
7 Poruks P, Yakubtsov I & Boyd J D, *Scr Mater*, 54 (2006) 41.
8 Gan C L, Liu X F & Xie J X, *Mater Sci Tech*, 29 (2013) 374.
9 Christy S, Pak H R & Meyers M A, *Metallurgical Application of Shock-Wave and High-Strain-Rate Phenomena*, (Marcel Dekker: New York), (1986), 835.
10 Gnyusov S F, Rotshtein V P, Polevin S D & Kitsanov S A, *Russ Phys J*, 53 (2010) 1046.
11 Rudd R E & Belak J F, *Comput Mater Sci*, 24 (2002) 148.
12 Allain S, Chateau J P, Bouaziz O, Migot S & Guelton N, *Mater Sci Eng A*, 387 (2004) 158.
13 Adler P H, Olson G B & Owen W S, *Metall Mater Trans A*, 17 (1986) 1725.
14 Ramalingam B, *Studies of bonding and void nucleation at inclusion-matrix interfaces in steel*. Pittsburgh, USA. 59-08 (1998).
15 Thomason P F, *Acta Metall Mater*, 41 (1993) 2127.